Electronic Supplementary Material (ESI) for Nanoscale.

Supporting Information

Investigating the magnitude and source of orientation-dependent interactions between TiO_2 crystal surfaces

Dongsheng Li*, Hailong Wang, Dongdong Xiao, Miao Song, Benjamin Legg, and Jaehun Chun

* Corresponding author: dongsheng.li2@pnnl.gov

This file includes:

- Supplementary Text
- Figures. S1 to S8
- Tables S1 to S5
- Equations S1 to S5
- References

Supplementary Text

Experimental

Tip fabrication: Crystallographically oriented face-specific atomic force microscopy (AFM) "TiO_2 rutile tips" with (001) plane used as force probe were fabricated by focus ion beam milling (Helios NanoLab 600i, FEI, Hillsboro, Oregon). The brief fabrication procedure is described as follows. A bulk TiO_2 plate with (001) facet was glued to the sample stage. Before milling, a layer of Al was deposited on rutile (001) surface using an e-beam evaporator (Telemark, TT-6, Washington) to avoid Ga ion contamination. The [001]-oriented TiO_2 tip was cut carefully from a specific area so that the edges were parallel to corresponding <100> direction (Figure 1A). The rutile pillar with size of ~(150 – 700) nm × (150 – 700) nm and height of 5-7 μm was obtained via focus ion beam cutting and then mounted to AFM cantilever end via Pt deposition (Figure 1B). The cantilever has spring constant ranging from 30-100 N/m. The angle between the (001) surface of TiO_2 pillar and the cantilever can be controlled and is 11° ±1°, which is required to maintain near parallel face-to-face contact between AFM TiO_2 tip and substrate. A small angle (i.e., 1°) deviation may still lead to comparable differences between effective contact area and tip surface area. To eliminate the effect of contact area, we quantified the effect of in-plane angular mismatch on TiO_2 (001)-TiO_2 (001) adhesion force by presenting the ratio of forces. Before force measurement, Al protective layer was removed with HCl solution in order to expose the TiO_2 (001) plane (Figure 1C).

AFM dynamic force spectroscopy (DFS) force measurement: Another rutile single crystal as substrate was mounted on a rotation stage which was fixed onto the AFM substrate holder. After mounting the substrate onto the rotation stage and loading TiO_2 tip into the cantilever holder with care, the crystallographic matching between two surfaces was established visually by rotating the stage until the edges of both substrate and tip were almost aligned (Figure 2A). Consequently, the error of mismatch angle between tip and substrate can be controlled to be less than ±5°.

Adhesion interaction forces were obtained by the deflection and the spring constant of the cantilever. The spring constants of all cantilevers were calibrated by the thermal fluctuation method.[1] Force measurements were performed with a commercial AFM (MFP3D, Asylum Research, Santa Barbara, California). A few nN force was applied on the tip when the tip and substrate were brought into contact and the system dwelled at this position for 1 second. The value of the retract velocity was changed after every approach/retract cycle to acquire the distribution of the rupture forces at different retract velocities ranging from 19 to 132 nN/s while approaching velocity was kept constant. Approximately 50-100 measurements were measured at each retract velocity. The substrate was rotated from 0° to 180° while orientation of the AFM cantilever with crystal as tip was fixed. The measurements presented were performed with a spring constant of ~600-800pN/nm in water at room temperature. All chemicals were purchased from Sigma Aldrich, St. Louis, Missouri. The pH for water was approximately 5.5-5.7. Figure S1 shows the average and three sets of experimental data.

High resolution AFM image, amplitude modulated AFM force curve measurement, and lattice averaged AFM image

Atomic force microscopy images and force curves were obtained using a Cypher ES microscope (Asylum Research) using an Arrow-UHF-AuD probe (NanoWorld) with a silicon tip, nominal tip radius of 10 nm, and nominal force constant of 1-6 N/m. The cantilevers displayed a resonance frequency of 200-400 KHz in water. Probe and cantilever holder were cleaned using ACS reagent grade isopropyl alcohol and air-dried prior to sample mounting. Sample was cleaned using argon-oxygen plasma and rinsed with high-purity water prior to imaging. Sample was characterized under air-equilibrated ACS reagent grade water (EMD-Millipore, OmniTrace Ultra). Approximately 200-400 μl of pure water was placed on the TiO_2 (001) surface, which was placed on AFM substrate holder in a sealed chamber of the AFM. The lateral thermal drift rate was reduced to be less than 1 nm/min. The force curves were collected at amplitude modulated mode, where set point was 1mV to 10 mV.

Initial lattice-resolution images were obtained by repeated-scanning of a 7.5 nm x 30 nm region in amplitude-modulated imaging modes (resolution of 0.56 Angstrom/pixel). The stack-averaged image was obtained by performing a median-filter operation on each image, then coaligning 60 sequential images of the using the FIJI StackReg plugin[2] and averaging these images. An affine transform was used in order to utilize both up-scans and down-scans, which are slightly distorted relative to each other due to image drift effects. Slight deviations of the lattice-averaged image from twofold symmetry are believed to be imaging artifacts.

The lattice average image was obtained by applying custom Python code to the stack-average image. In this code, autocorrelation methods were applied to identify the fundamental lattice-translation vectors. These translation vectors were then used to map the crystal onto itself and generate an averaged image of the basic unit cell, incorporating a total of 1132 distinct unit cells to significantly reduce noise.

Coincident site lattice theory

The several other reproducible maxima (i.e., ~ ±30º) and small minima (i.e., at ~ ±15°) (Figure S1) were due to the superlattice pattern formation between two surfaces at θ =36.9º, where certain atoms were at coincident sites (Figure S3b). This was consistent with coincident site lattice theory, where $\Sigma 1$ (θ=0º and 90º) corresponds to the lowest energy configuration for a square lattices and $\Sigma 5$ (θ=36.9º, it was easily seen by rotating two square lattices on top of each other) corresponds to a relatively lower energy configuration. The small angle discrepancy between our experimental ~30º and theoretical 36.9º was probably due to 10º rotation step and effect of water layer between two TiO_2 surfaces.

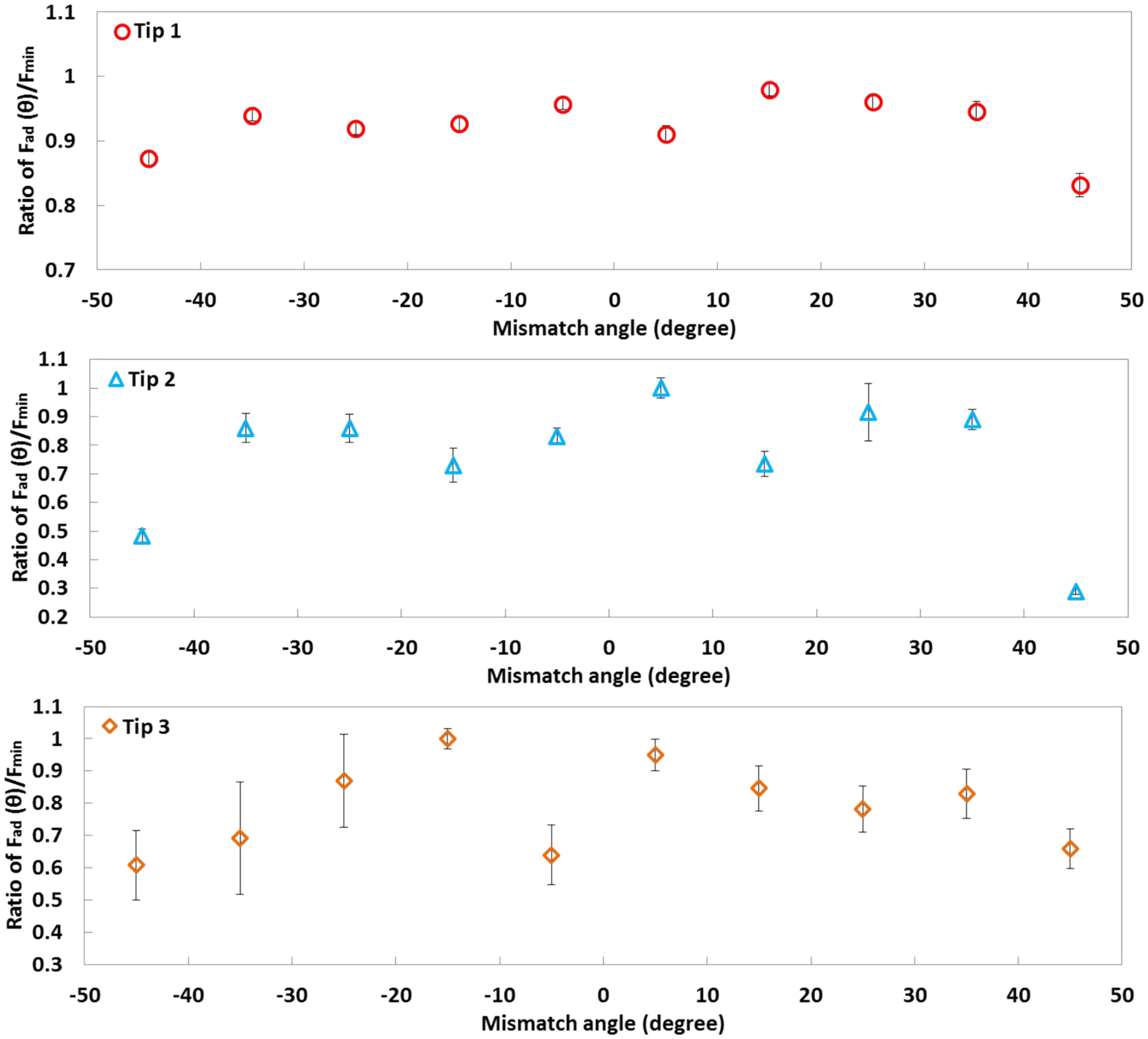

Figure S1. Three sets of experiment results of the change in ratio of F_{ad}/F_{max} as a function of lattice mismatch angle between two rutile TiO_2 (001) plane at the retracting rate of 100nm/s from Tip 1, 2, and 3 in which the adhesive force F_{ad} is normalized to the measured maximum force F_{max}. Error bar is the standard error of the mean. The rotation step was 10º, and the angle was shifted 5º from the measurement angle to standardize the plot.

Macroscopic geometric effects with respect to tip-shape and alignment

Changes in contact geometry might result due to variations in tilting of the substrate (001) surface relative to the probe (001) surface. Such misalignments are known to influence surface adhesion[3]. In order to minimize the effect of contact geometry, we carefully aligned substrate and the rutile tip holder to be in a horizontal position and parallel to each other.

Our previous mica (001) - mica (001) interaction results obtained by the same method have shown 60 °periodicity with a square shape tip, indicate that the tip shape and alignment does not affect the periodicity measurement.

Effective contact area

Although the tip surface was fabricated at an ~11° angle with the cantilever, the tip surface may not have been perfectly parallel to the substrate surface. The maximum effective contact area was tip surface area. Because the effective contact area was unknown and even a small angle between tip and substrate surfaces would bring appreciable changes in adhesion forces, key results were presented as the ratio of forces to eliminate possible uncertainties from an assumption that the effective contact area was more or less constant for each crystal tip in each set of force measurements.

For example, when the two surfaces have 1–2° tilt from each other in both the *x* and *y* directions (Figure S2 shows 1–2° tilt along one direction), at a separation less than 1 nm, the effective contact area ranges from ~200 nm^2 to ~800 nm^2, regardless of the tip size (Table S1). We only considered the area for separations smaller than 1 nm (up to 2 layers of water on each surface) because the calculated adhesion force at separation of 1 nm based on DLVO is ~10^6 N/m^2, which was comparable with the measured adhesion force ($10^6 N/m^2$, based on tip surface area). The force applied on the mica tip was a few nN, leading to a pressure of 10^5 N/m^2 based on tip surface area and 10^7 N/m^2 based on effective contact area, which was comparable to the pressure needed to penetrate the hydration layer.

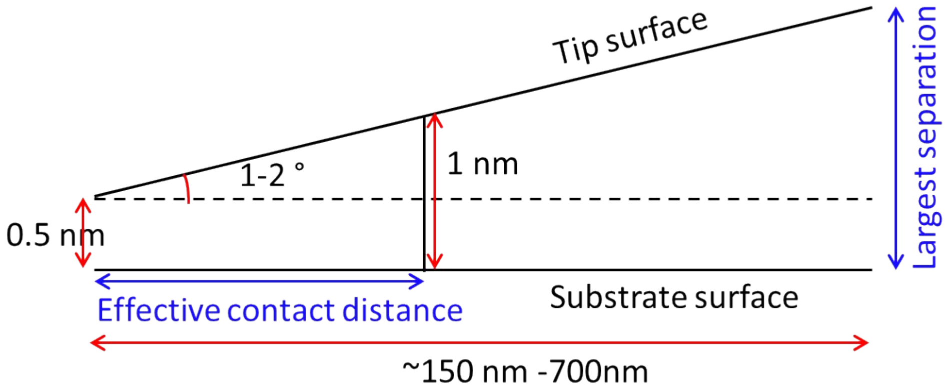

Figure S2. A schematic diagram of a side view of the tip surface contacting the substrate surface.

Table S1. Effective contact area calculation based on 1–2° difference from parallel. (Effective separation <1 nm, up to 4 layers of water.)

Tip size (nm)	**150**	**150**	**300**	**300**	**700**	**700**
Angular deviation (°)	1.00	2.00	1.00	2.00	1.00	2.00
Smallest separation (nm)	0.5	0.5	0.5	0.5	0.5	0.5
Largest separation (nm)	2.61	5.23	5.23	10.46	12.21	24.41
Effective contact distance (nm)	28.66	14.33	28.66	14.33	28.66	14.33
Effective contact area (nm^2)	**821.70**	**205.55**	**821.70**	**205.55**	**821.70**	**205.55**

Estimation of separation between two rutile (001) surfaces

Based on previous frequency modulated AFM force curves on the TiO_2 (110) surface and the size of the tip used in the force measurement[4], the pressure necessarily to penetrate hydration layers absorbed on the TiO_2 surface was estimated in the order of 10^{6-7} N/m^2, whereas the externally applied force (F_{app}) by the AFM rutile tip was approximately 10^{5-7} N/m^2 based on tip surface and effective contact area (see SI for details). It seems likely that two layers of water (one layer of water on each TiO_2 surface, if the F_{app} is in the order of 10^{6-7} and can penetrate one layer of water), and possibly up to four layers (two layers of water on each TiO2 surface, if F_{app} is in the order of 10^5 cannot penetrate absorbed water layers at all) remain between the two rutile surfaces when they are in contact.

Interaction energy and force calculation in vacuum

The Matsui-Akaogi potential (1) was used to describe the atomic interactions in rutile. This force field can accurately reproduce the lattice energy, polymorphic, elastic and dielectric constant, and relative energies of $TiO_{2.}$[5] The interaction energy U between atoms i and j can be expressed as,

$$U_{ij} = A_{ij}\exp\left(-\frac{r_{ij}}{\rho_{ij}}\right) - \frac{C_{ij}}{r_{ij}^6} + \frac{q_i q_j}{r_{ij}} \qquad (S1)$$

Here r_{ij} is the between atom i and j. The partial charges q is $+2.196$ and -1.098 for Ti and O atom, respectively[6] In addition to the electrostatic term, the first two terms in Eq. S1 constitute a Buckingham potential. The parameters for the Buckingham potential are listed in Table S1.[7]

Table S2. Parameters for the Buckingham potential of the Matsui-Akaogi Force Field[7]

ion-ion	A_{ij} (kcal/mol)	ρ_{ij} (Å)	kcal (Å^6/mol)
Ti-Ti	717654	0.154	120.997
Ti-O	391053	0.194	290.392
O-O	271719	0.234	696.941

To calculate intrinsic forces, we took two identical rutile crystals with (001) surfaces and rotate the bottom crystal by $-\theta/2$ and the top crystal by $\theta/2$ about the [001] direction (z-axis) (Fig. S2). The misorientations range $0 < \theta < 180^o$ was considered due to the 2-fold symmetry of rutile crystal structure about the [001] direction. We could further reduce that range to $0 < \theta < 90^o$because the equivalent misorientated surfaces were generated for clockwise and counterclockwise rotations. To model the macroscopic AFM tip and substrate, we applied in-plane periodic boundary conditions for the simulation cell in x and y directions. The misorientation, θ, and simulation box sizes, (l_1, l_2, l_3), must satisfy the following conditions: $\tan(\theta/2) = n_2/n_1$ $l_1 = l_2 = \left(n_1{}^2 + n_2{}^2\right)^{1/2}a, l_3 = n_3 c$, where n_1, n_2, n_3 are integers and a, c are the lattice constants of rutile. These integers were chosen to ensure the sizes of each crystal were at least twice the cut-off radius of the force field to avoid the interactions between periodic boundaries (x and y directions) and surfaces (z direction). We chose the misorientations with low values of (m, n): (1, 0), (1, 1), (2, 1), (3, 1).[5,12,] During the relaxation process, the top and bottom layers were fixed with thickness more than the cut-off radius (dashed green boxes in Fig. S2). The detailed information for computation cells (blue boxes) with various misorientation $\theta = 0 - 90^o$ are listed in Table 1.

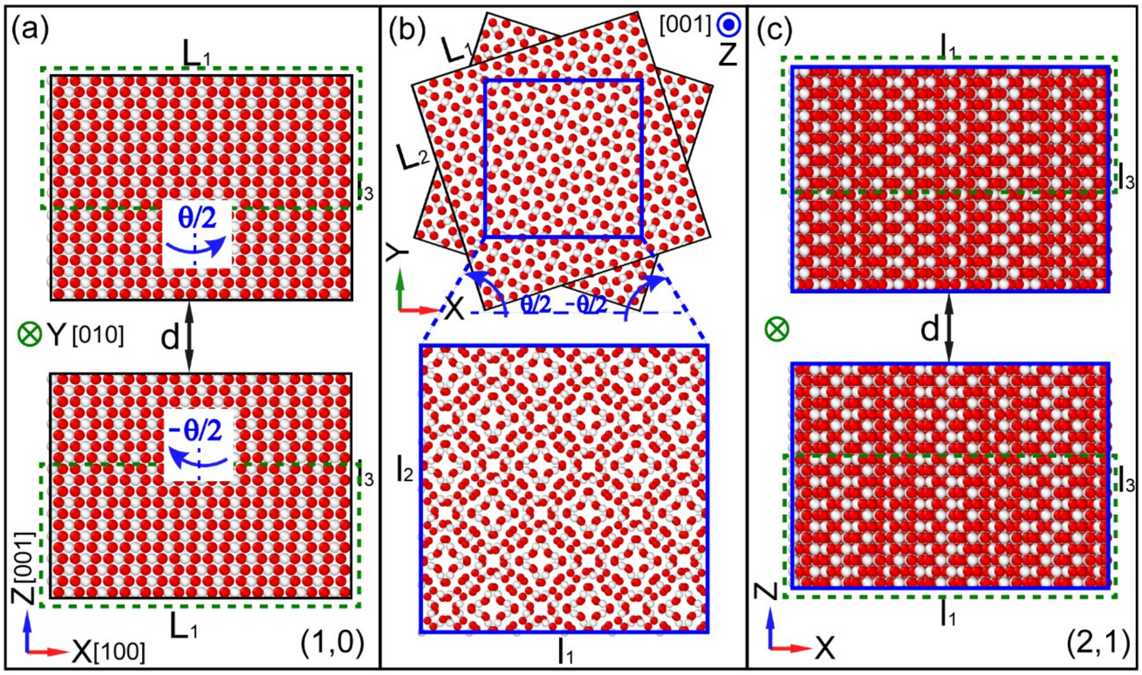

Figure S3. (a) Side view of two identical rutile single crystals with (001) surfaces at separation, $d = 10\text{Å}$ before rotation. Red, green, and blue arrows indicate x, y, and z directions. (b) Top view of top and bottom crystals with rotation $\theta/2$ and $-\theta/2$ about [001] direction, respectively. Misorientation, $\theta = 36.9^o$, and box dimensions (l_1, l_2) satisfy $\tan(\theta/2) = n_2/n_1$ and $l_1 = l_2 = \left(n_1{}^2 + n_2{}^2\right)^{1/2}a$. Here $n_1 = 3$ and $n_1 = 1$. (c) Side view of computation cell with misorientation $\theta = 36.9^o$ and dimensions $(l_1,l_1,l_3) = (42.62, 42.62, 30.33)$ Å after rotation.

Table S3. Atomic model with various misorientation θ.

(n_1,n_2)	θ	(l_1,l_2,l_3) (Å)	atom number
(1, 0)	0^o	(40.44, 40.44, 30.33)	9720
(1, 1)	90^o	(44.48, 44.48, 30.33)	11760
(2, 1)	53.1^o	(40.19, 40.19, 30.33)	9600
(3, 1)	36.9^o	(42.62, 42.62, 30.33)	10800

Van der Waals interaction

Then we calculated the non-bonded interaction energy only (van der Waals energy, Figure S4 a), as function of separation, d, for each misorientation, θ.

$$\gamma_{vdW}(\theta,d) = \frac{1}{l_1 l_2}(U_{vdW}(\theta,d) - U_{vdW}(\theta,\infty)) \qquad (S2)$$

Here $U_{vdW}(\theta,\infty)$ is the reference van der Waals energy for two crystals without interaction. The interaction or force between two surfaces in Figure S4 b can also be directly derived from $\sigma_{vdW}(\theta) = \frac{\partial \gamma_{vdW}(\theta,d)}{\partial d}$. There are two maximum interaction at misorientations θ=0 and θ=2/π for non-bonded interaction: $\sigma_{vdW}^{max}(0)/\sigma_{vdW}^{min}(\theta) = 1.4$ and $\sigma_{vdW}^{max}(0)/\sigma_{vdW}^{min}(\pi/2) = 1.05$. The two fold symmetry of van der Waals interaction is results from the 2-fold symmetry of O atoms because the non-bonded O-O force are dominant in the van der Waals interaction.

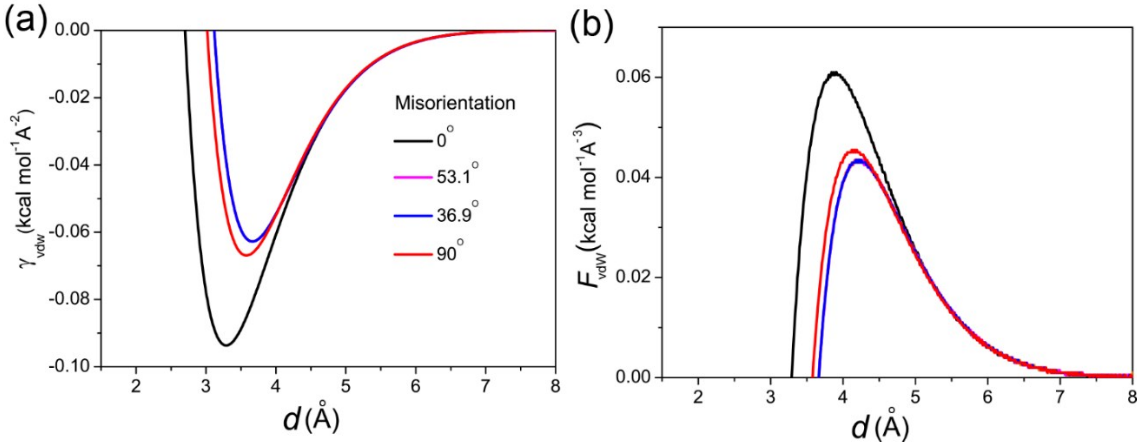

Figure S4. The van der Waals interaction energy, γ_{vdW} (a) and interaction F_{vdW} (b) as function of separation, d, for misorientation, $\theta = 0 - 90^o$.

There are several factors that can affect the adhesive force between TiO_2 surfaces, including interatomic Coulombic and van der Waals interactions, selective adsorption of solvent molecules, and hydration forces. Our force curve measurements were taken at a pH of 5.5-5.7, which corresponds to the isoelectric point of the TiO_2 (001) surface[8] and hence electrostatic interaction can be negligible. In vacuum, the interatomic Coulombic interaction is believed to be the primary driving force for OA.[9] However, this interaction experiences screening due to the absorbed water on surface.[9] Molecular dynamic simulation showed that the van der Waals interaction exhibited a twofold symmetry due to the twofold symmetry of O atoms (Figure S4). These factors raise the question of what role hydrogen bonding at the surfaces plays in OA of rutile nanocrystals.

Two (001) Rutile surfaces with water molecules dissociation

The adhesive force between crystal surfaces are affected by not only the intrinsic forces in vacuum but also the selective adsorption and surface chemistry of liquid-phase molecules at surface-liquid interface, and solvent-mediated interaction.[7] To calculate the intrinsic forces in vacuum, we took two identical rutile single crystals with (001) surfaces and rotated the bottom crystal by $-\theta/2$ and the top crystal by $\theta/2$ about the

[001] direction (z-axis) (Figure S5). The misorientations range $0 < \theta < 180^o$ was considered due to the twofold symmetry of rutile crystal structure about the [001] direction. We could further reduce that range to $0 < \theta < 90^o$ because the equivalent misorientated surfaces were generated for clockwise and counterclockwise rotations. To model the macroscopic AFM tip and substrate, we applied in-plane periodic boundary conditions for the simulation cell in x and y directions. The misorientation, θ, and dimensions of each slabs, (l_1, l_2, l_3), had to satisfy the following conditions: $\tan(\theta/2) = n_2/n_1$, $l_1 = l_2 = (n_1{}^2 + n_2{}^2)^{1/2}a,\ l_3 = n_3c$, where n_1, n_2, n_3 are integers and a, c are the lattice constants of rutile at room temperature. These integers were chosen to ensure the sizes of each crystal were at least twice the cut-off radius of the force field (12.66Å) to avoid the interactions between periodic boundaries (x and y directions). We chose the misorientations with low values of (n_1, n_2): (1, 0), (1, 1), (2, 1), (3, 1).[5,12] Rutile (001) surface is very reactive and favors dissociative adsorption than other major low-indexed surfaces, with the formation of two surface hydroxyls.[10] In Figure S5a, one terminal hydroxyl (O_T-H_T, orange-blue) from water binds to a surface Ti atom (white) via its terminal oxygen (orang), and a bridging hydroxyl (O_B-H_B, magenta-cyan), in which the hydrogen (H_B, cyan) in water randomly binds to one of two bridging (2-fold coordinated) surface oxygen (O_B, magenta). The details information for computation cells (blue boxes in Figure. 5b) of two rutiles slabs with water molecular dissociation for various misorientation $\theta = 0 - 90^o$ are listed in Table S1.

After surface relaxation, the unsaturated bridging surface oxygen (O, red) interacts with the hydrogen (H_T, blue) in terminal hydroxyl (O_T-H_T, gold-blue) in the insert of Figure S5 a, which was consistent with the previous ab-initio calculations.[10]

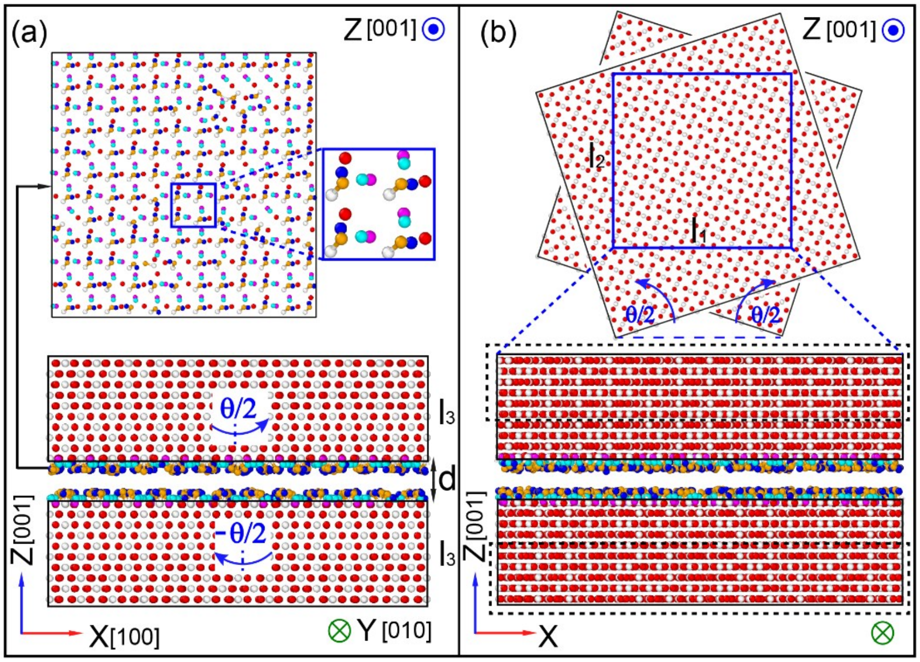

Figure S5. (a) Top and side views of two identical rutile single crystals with water dissociation on (001) surfaces. The separation between rutile surfaces $d = 6.5$Å. White, red, orange, magenta, blue, and cyan denote Ti, O, O_T, O_B, H_T, and H_B atom, respectively. Red, green, and blue arrows indicate x, y, and z directions. (b) Top and side view of top and bottom crystals with rotation $\theta/2$ and $-\theta/2$ about [001] direction, respectively. Misorientation, $\theta = 36.9^o$, and box dimensions (l_1, l_2) satisfy $\tan(\theta/2) = n_2/n_1$ and $l_1 = l_2 = (n_1{}^2 + n_2{}^2)^{1/2}a$. Here $n_1 = 3$ and $n_1 = 1$.

Table S4. Atomic model with various misorientation θ.

(n_1,n_2)	θ	(l_1,l_2,l_3) (Å)	rutile atoms	water atoms
(1, 0)	0^o	(53.91, 53.91, 17.67)	8640	864
(1, 1)	90^o	(50.83, 50.83, 17.67)	7680	768
(2, 1)	53.1^o	(60.28, 60.28, 17.67)	10800	1080
(3, 1)	36.9^o	(56.83, 56.83, 17.67)	9600	960

Intermolecular potentials for rutile and dissociated water dissociation on surfaces

In this study, the Matsui-Akaogi (MA) potential[11] was adopted to describe the atomic interactions of Ti and O atoms in rutile slabs. This force field can accurately reproduce the lattice energy, polymorphic, elastic and dielectric constant, and relative energies of TiO_2.[5] The interactions are described by a summation of a Buckingham potential for the van der Waals interactions and the Coulombic potential for the electrostatic interactions,

$$U_{ij} = A_{ij}\exp\left(-\frac{r_{ij}}{\rho_{ij}}\right) - \frac{C_{ij}}{r_{ij}^{6}} + \frac{q_i q_j}{r_{ij}} \qquad (S3)$$

Here r_{ij} is the between atom i and j. The partial charges q is +2.196(e), -1.098(e) for Ti, and O atom, respectively.[12] In addition to the electrostatic term, the parameters for the Buckingham potential (the first two terms in Eq. S1) are listed in Table S3.

Table S5 Interaction parameters of Buckingham potential for the MA Force Field[5]

ion-ion	A_{ij} (kcal/mol)	ρ_{ij} (Å)	C_{ij} (kcal mol^{-1} Å^6)
Ti-Ti	717647.4	0.154	121.0676
Ti-O, Ti-O_B	391049.1	0.194	290.3317
O-O, O-O_T, O-O_B	271716.3	0.234	696.8883
Ti-O_W	28593.02	0.265	148.000
Ti-O_T	315480.8	0.194	290.3317

The SPC/E water model[13] was chosen and interactions for water molecules have been treated as a combination of Lennard-Jones (LJ) interactions and a Coulomb term for electrostatic interactions,

$$U_{ij} = 4\varepsilon_{ij}\left[\left(\frac{\sigma_{ij}}{r_{ij}}\right)^{6} - \left(\frac{\sigma_{ij}}{r_{ij}}\right)^{12}\right] + \frac{q_i q_j}{r_{ij}} \qquad (S4)$$

Here the partial charges q is -0.8476(e), and +0.4238 (e) for O_W, and H_W atom, respectively.[12] Here O_W and H_W denote O and H atoms in water molecules. In addition to the electrostatic term, the parameters for the LJ potential (the first term in Eq. S2) are listed in **Table S4**.

Table S5 Interaction parameters for L-J potential[5]

ion-ion	ε_{ij} (kcal/mol)	σ_{ij} (Å)
O_W-O_W, O-O_W	0.15539	3.1660
O_T-O_T, O_T-O_B, O_B-O_B	0.15539	3.1660

To describe interactions between TiO_2 and water, Bandura and Kubicki (BK) adopted a hybrid force field combining elements of Eq. S1 and Eq. S2.[14] For molecular adsorption on TiO_2 surfaces, the potential was used to describe bonding between O_W and Ti (Table S3), and the interactions between O and O_W were equal to those between O_W and O_W of two water molecules (Table S4). In the BK potential, the partial charges for O and H atoms in terminal (O_T and H_T) and bridging (O_B and H_B) hydroxyl groups were -1.008(e), +0.459(e), -1.035(e), +0.486(e).[12] O_T and O_B interact with all O and Ti atoms of TiO_2 via the molecular adsorption potential, same with the interactions of O-Ti and O-O in rutile unless otherwise indicated (Table S3).[12] Note that the non-bonded interactions between O_B and O_T (O_B-O_T, O_B-O_T, O_T-O_T) were assumed to be same with those between O_W and O (Table S4). All remaining interactions were the same as those of molecular adsorption, including the LJ interactions for the O_B and O_T with water molecular as well as Coulombic interactions (Table S4).[12] The Ti-O_T/O_T-H_T bond lengths and Ti-O_T-H_T bond angles in terminal hydroxyl, as well as O_B-H_B bond length in bridging hydroxyl are fixed with parameters in Table S5. Bond-length and bond-angle constraints are enforced using the SHAKE algorithm.[15]

Table S6. Bond lengths and angles[5]

bond	Ti-O_T	O_T-H_T	O_B-H_B	bond	Ti-O_T-H_T
length (Å)	1.895	0.983	0.994	Angle (°)	90.85

The molecular dynamics simulations were performed via LAMMPS program package[16] at room temperature (300 K) using a time step 1fs. The two crystals were first positioned $d = 6.52\text{Å}$ apart from each other and equilibrated using Berendsen thermal bath[17] for 10 ps. The vertical atomic positions of atoms in top and bottom layers (in dashed boxes of Figure S5) were "frozen" to control the separation between slabs, while the translation shift between two slabs was allowed. After surface relaxation, the unsaturated bridging surface oxygen (O, red) interacted with the hydrogen (H_T, blue) in terminal hydroxyl (O_T-H_T, orange-blue) in insert of Figure S5a shows that, which was consistent with the previous ab-initial calculations.[10] Then we moved the top slab approximately 3.6 Å downward at a constant speed of 10m/s (36 picoseconds of simulation time), and then the entire system equilibrated with separation $d = 2.92\text{Å}$ for 10ps. Figure S6 and S7 show the atomic configuration of two equilibrated rutile slabs with surface water dissociation for various misorientation. We immediately saw the formation of a network of hydrogen bonds between the O_H (orange) in bridging hydroxyls on one surface and the H_B (cyan) in bridging hydroxyls of the other surface. The regular atomic-scale patterns at 0^o and 90^o indicate that 0° and 90° mismatch orientations are favorable for hydrogen bonds formation.

Comment [LD]:

Comment [LD]:

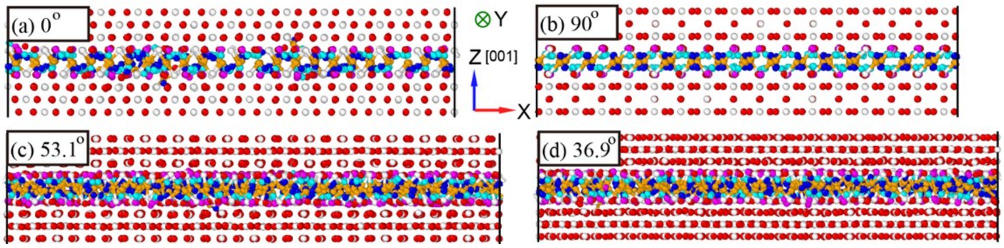

Figure S6. Side view of two rutile slabs with water dissociation on (001) surfaces with separation $d = 2.92\text{Å}$ for misorientation $\theta = 0^o$ a), 90^o b), 53.1^o c), and 36.9^o d).

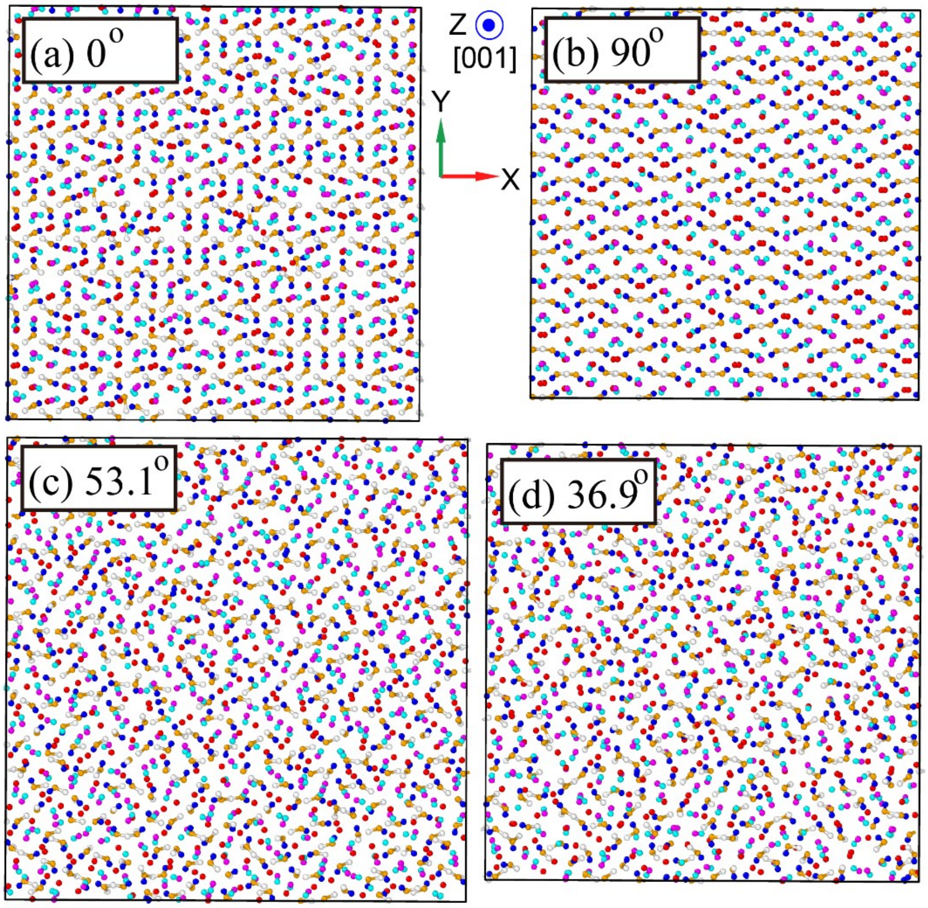

Figure S7. Top view of two rutile slabs with water dissociation on (001) surfaces with separation $d = 2.92\text{Å}$ for misorientation $\theta = 0^o$ a), 90^o b), 53.1^o c), and 36.9^o d).

After the formation of a network of hydrogen bonds, the top slab was retracted upwards at a constant speed of 10m/s to the initial separation, $d = 6.52\text{Å}$. For a given separation distance, the interaction force was calculated as the sum of all individual forces acting on the atoms of one rutile slab as well as dissociated water molecule on surface. We expected the maximum amplitude of interaction force (adhesive forces) for 0^o and 90^o to be higher than those for 53.1^o and 36.9^o, because the regular organization of hydrogen bonds network is more sufficient to reduce interaction energy. The interaction force per unit area, $\sigma(\theta,d)$, as function of separation, d, for each misorientation, θ, is shown in Figure 4 (solid lines)**.** As we retracted the top slab for all the misorientations, the interaction forces first increased, then reached the adhesive forces, and finally decreased with increasing separation. There were two obvious maximums of adhesive forces at misorientations $\theta = 0°$ and $90°$, corresponding to the single- and twinned-crystal structures. Our results were consistent with the assembly of anatase nanocrystals into single or twinned crystal via oriented attachment (OA) in the previous experiments[18] and atomic simulations.[7, 19] The fourfold symmetric adhesive force between (001) rutile surfaces with water dissociation resulted from the fourfold symmetry of O_T-H_B pairwise interactions, where O_T binds to Ti on one surface and H_B binds to bridging O_B on other surface.

The dissociated water passivated the two surfaces and prevented their aggregation into single- and twinned-crystal structures at room temperature. The network of hydrogen bonds between surfaces formed from water absorption played an important role in OA of nanocrystals.[7, 19] The anisotropy of F_{ad} can be calculated as: $F_{ad}(0°)/F_{ad}(36.9°) = 2.4$ and $F_{ad}(90°)/F_{ad}(36.9°) = 2.5$ around ~4 Å (Figure 4), which is a bit higher than our experimental measurement (1.04-1.4 for $F_{ad}(0°)/F_{ad}(\sim35°)$). Besides the effect contact area deviation as discussed previously, a possible reason would be additional water layers (i.e., more than one layer of absorbed water on each rutile surface considered in the current simulations), which would also be related to hydration forces.

We acknowledge that the experimental data shows a few sharp minima cusps in binding at ± 45° with a relatively insensitive adhesive force for intermediate values between ± 30°. However, because the computational simulations cannot calculate the interaction force at a random mismatch angle, it can't calculate F_{ad} (min) or the ratio of F_{ad} (min) to F_{ad} (max). Current results suggest a sharp maximum in the binding strength at 0° and 90°, with a relatively insensitively minimum-binding energy between 37° and 53°.

Interaction of two rutile surface without water adsorption in vacuum

To highlight the influence of hydrogen bonds network on surface interaction, we also calculated the interaction of two rutile surfaces without water adsorption in a vacuum using the same approaching and retracting simulations. For the same misorientation, it was clear that the rutile surfaces with water dissociation had longer adhesive distances (d_{ad}, which is defined as the surface separation associated with the maximum attractive forces between surfaces) and lower adhesive force, in contrast to their behavior in a vacuum (Figure S8) . The dissociated water passivated the two surfaces and prevented their aggregation into single- and twinned-crystal structures at room temperature. The network of hydrogen bonds between surfaces formed from water absorption played an important role in OA of nanocrystals.[7, 19]

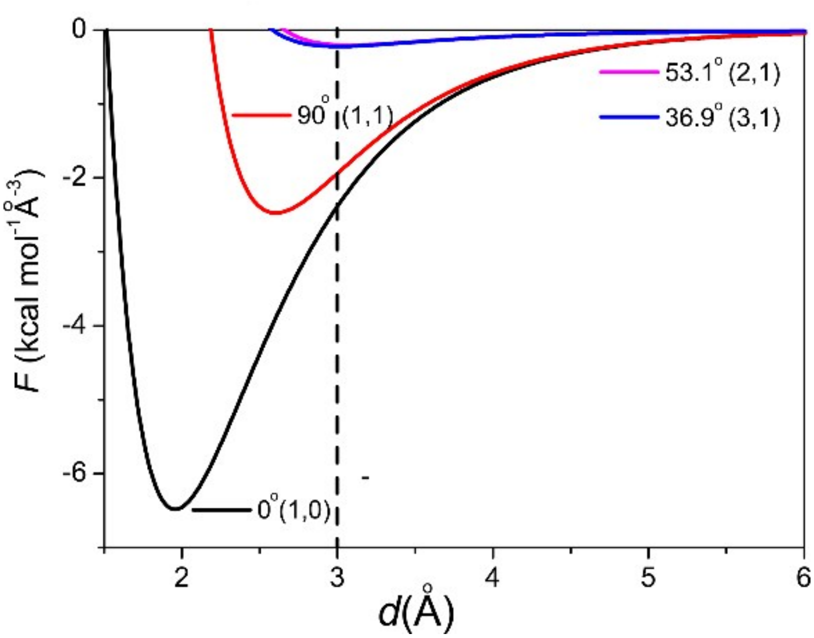

Figure S8. The interaction force per unit area, *F* (*θ, d*), in vacuum without water as function of *d*, for misorientation, *θ* = 0-90º.

An orientation-dependent macroscopic dispersion force

While a conventional Lifshitz theory assumes a scalar dielectric response of material, the lattice structure of TiO_2 would bring a tensorial nature of dielectric responses, reflecting the fourfold symmetry of TiO_2 crystal. Similar to our previous study,[20] the orientational nature of the dispersion force can be qualitatively estimated by subsequent nature of Hamaker constant $\mathrm{A} = \mathrm{A}_0 + \mathrm{A}_1(1 + 2\cos^2\theta)$ where A_0 and A_1 denote non-angular and angular factors which are functions of dielectric properties of TiO_2 and water. Here θ is the in-plane mismatch angle between TiO_2 surfaces. The fourfold symmetry of TiO_2 (i.e., every 90° should be optically identical) suggests that the factor becomes $1 + 2\cos^2(4\theta)$, which qualitatively explains the orientational dependence. However, an exact non-local dielectric response of TiO_2 is required to perform further quantitative analysis (such as the dominance of A_0 over A_1 and determination of the ratio of forces).

DLVO forces

The force measurements were taken at a pH of 5.5-5.7 which corresponded to the isoelectric point (iep) of the TiO_2 (001) surface[8] and hence the electrostatic interaction between the TiO_2 surfaces can be negligible to calculate the forces based on DLVO theory.

For van der Waals forces per area, (F_{vdW}), a continuum-based approach based on the Hamaker constant can be used as the first approximation:

$$F_{\mathrm{vdW}} = -\frac{A}{6\pi h^3} \qquad \text{(S5)}$$

where A is the Hamaker constant. A value for A was reported to be ~5.35×10^{-20} J for TiO_2–water– TiO_2.[21] While the discrete nature of the solvent (i.e., water) was shown to significantly increase the Hamaker constant for TiO_2-water-TiO_2,[22] it was not considered due to the uncertainty associated with the formulation to implement the discrete nature at separations of interest in this study. Therefore, the reported value was used as a simple estimate, although Equation (S5) would be a simple and first approximation for van der Waals forces at such small separations.[22]

REFERENCES

1. J. L. Hutter and J. Bechhoefer, *Review of Scientific Instruments*, 1993, **64**, 1868.
2. P. Thevenaz, U. E. Ruttimann and M. Unser, *IEEE transactions on image processing*, 1998, **7**, 27-41.
3. A. Çolak, H. Wormeester, H. J. Zandvliet and B. Poelsema, *Applied surface science*, 2012, **258**, 6938-6942.
4. T. Hiasa, K. Kimura, H. Onishi, M. Ohta, K. Watanabe, R. Kokawa, N. Oyabu, K. Kobayashi and H. Yamada, *Japanese Journal of Applied Physics*, 2009, **48**, 08JB19.
5. D. Collins and W. Smith, *Council for the Central Laboratory of Research Councils, Daresbury, UK*, 1996.
6. J. G. Traylor, H. Smith, R. Nicklow and M. Wilkinson, *Physical Review B*, 1971, **3**, 3457.
7. K. A. Fichthorn, *Chemical Engineering Science*, 2015, **121**, 10-15.
8. J. W. Bullard and M. J. Cima, *Langmuir*, 2006, **22**, 10264-10271.
9. H. Zhang and J. F. Banfield, *CrystEngComm*, 2014, **16**, 1568-1578.
10. Z.-Y. Zhao, *The Journal of Physical Chemistry C*, 2014, **118**, 4287-4295.

11. M. Matsui and M. Akaogi, *Molecular Simulation*, 1991, **6**, 239-244.
12. M. Předota, A. Bandura, P. Cummings, J. Kubicki, D. Wesolowski, A. Chialvo and M. Machesky, *The Journal of Physical Chemistry B*, 2004, **108**, 12049-12060.
13. H. Berendsen, J. Grigera and T. Straatsma, *J. phys. Chem*, 1987, **91**, 6269-6271.
14. A. Bandura and J. Kubicki, *The Journal of Physical Chemistry B*, 2003, **107**, 11072-11081.
15. J.-P. Ryckaert, G. Ciccotti and H. J. Berendsen, *Journal of Computational Physics*, 1977, **23**, 327-341.
16. S. Plimpton, *Journal of computational physics*, 1995, **117**, 1-19.
17. H. J. Berendsen, J. v. Postma, W. F. van Gunsteren, A. DiNola and J. Haak, *The Journal of chemical physics*, 1984, **81**, 3684-3690.
18. R. L. Penn and J. F. Banfield, *Science*, 1998, **281**, 969-971.
19. M. Raju, A. C. Van Duin and K. A. Fichthorn, *Nano letters*, 2014, **14**, 1836-1842.
20. D. Li, J. Chun, D. Xiao, W. Zhou, H. Cai, L. Zhang, K. M. Rosso, C. J. Mundy, G. K. Schenter and J. J. D. Yoreo, *Proceedings of the National Academy of Sciences, under review*.
21. L. Bergström, *Advances in Colloid and Interface Science*, 1997, **70**, 125-169.
22. J. Chun, C. J. Mundy and G. K. Schenter, *The Journal of Physical Chemistry B*, 2015, **119**, 5873-5881.